

# Enzyme-Mimic Peptide Assembly To Achieve Amidolytic Activity

Yoke-Ming Wong,<sup>†,‡</sup> Hiroyasu Masunaga,<sup>‡</sup> Jo-Ann Chuah,<sup>†</sup> Kumar Sudesh,<sup>#</sup> and Keiji Numata<sup>\*,†</sup>

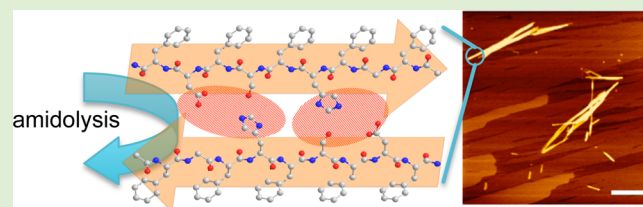
<sup>†</sup> Enzyme Research Team, RIKEN Center for Sustainable Resource Science, 2-1, Hirosawa, Wako-shi, Saitama 351-0198, Japan

<sup>‡</sup> Japan Synchrotron Radiation Research Institute, 1-1-1, Kouto, Sayo-cho, Sayo-gun, Hyogo 679-5198, Japan

<sup>#</sup> Ecobiomaterial Research Laboratory, School of Biological Sciences, Universiti Sains Malaysia, 11800, Minden, Penang, Malaysia

## Supporting Information

**ABSTRACT:** Amyloid fibers are classified as a new generation of tunable bionanomaterials that exhibit new functions related to their distinctive characteristics, such as their universality, tunability, and stiffness. Here, we introduce the catalytic residues of serine protease into a peptide catalyst (PC) via an enzyme-mimic approach. The rational design of a repeating pattern of polar and nonpolar amino acids favors the conversion of the peptides into amyloid-like fibrils via self-assembly. Distinct fibrous morphologies have been observed at different pH values and temperatures, which indicates that different fibril packing schemes can be designed; hence, fibrillar peptides can be used to generate efficient artificial catalysts for amidolytic activities at mild pH values. The results of atomic force microscopy, Raman spectroscopy, and wide-angle X-ray scattering analyses are used to discuss and compare the fibril structure of a fibrillar PC with its amidolytic activity. The pH of the fibrillation reaction crucially affects the  $pK_a$  of the side chains of the catalytic triads and is important for stable fibril formation. Temperature is another important parameter that controls the self-assembly of peptides into highly stacked and laminated morphologies. The morphology and stability of fibrils are crucial and represent important factors for demonstrating the capability of the peptides to exert amidolytic activity. The observed amidolytic activity of PC4, one of the PCs, was validated using an inhibition assay, which revealed that PC4 can perform enzyme-like amidolytic catalysis. These results provide insights into the potential use of designed peptides in the generation of efficient artificial enzymes.



## INTRODUCTION

Enzymes are highly efficient and selective catalysts of reactions in living systems, which present unique catalytic microenvironments.<sup>1</sup> An artificial catalyst was first fabricated to simulate and understand the relationships between enzyme structures and functions and explore how the uniqueness of enzymes contributes to their high catalytic efficiency.<sup>2,3</sup> Research into the pragmatic use of artificial catalysts has slowly expanded to the preparation of inexpensive, stable, and highly efficient catalysts as a method of overcoming the limitations of natural enzymes, such as heat instability, incompatibility with organic solvents, and so on.<sup>4,5</sup> In recent decades, different types of artificial catalysts, including cyclodextrin,<sup>6,7</sup> metal complexes,<sup>8</sup> macromolecular scaffolds (such as crown ether<sup>9</sup> and porphyrins<sup>10</sup>), polymers,<sup>11</sup> and biomolecules (such as peptides<sup>12,13</sup> and antibodies<sup>14</sup>), have been explored and constructed to mimic the catalytic capabilities and fine structures of natural enzymes through various approaches.

Although several of the previously fabricated artificial catalysts have exhibited significant efficiency and selectivity, certain disadvantages still remain in these designs, including complicated synthetic routes, low productivity, and poor cooperativity between the catalytic centers and substrates.<sup>15</sup> Among the disadvantages, the structural cooperativity of natural enzymes plays a prominent role in determining the catalytic efficiency of artificial catalysts.<sup>16</sup> Atassi and Manshouri designed

and synthesized a 29 amino acid, cyclic peptide-based artificial catalyst and showed the catalytic capabilities of precise molecular mimics of trypsin and  $\alpha$ -chymotrypsin.<sup>12</sup> Although the attempts to reproduce the catalytic activities of cyclic peptides were not completely successful, the findings indicated that poor conformational stability may have led to the poor cooperativity between the catalytic centers and substrates.<sup>12</sup> This finding emphasizes the pivotal importance of conformational stability between catalytic centers and binding sites, which is a remarkable insight into the design and redesign of artificial catalysts.

Amyloid fibers are generally composed of  $\beta$ -sheet structures that are oriented perpendicularly to the fibril axis, connected via a dense hydrogen-bonding network, and eventually elongated to form supramolecular nanostructures with widths of 8–30 nm and lengths of up to several micrometers.<sup>17–19</sup> Although they first received attention as pathological entities, scientists have classified amyloid fibers as a new generation of tunable bionanomaterials with multiple functions related to the distinctive characteristics of amyloid fibers.<sup>17,20</sup> Amyloid fibers are also intriguing with regard to the design of our artificial catalyst.<sup>21</sup> Currently, amyloid fibers have been functionalized

Received: July 31, 2016

Revised: September 13, 2016

Published: September 19, 2016

for applications in drug delivery,<sup>22</sup> environmental carbon dioxide capture,<sup>23</sup> enzyme immobilization,<sup>25</sup> and enzyme-like catalysis.<sup>24</sup> Rufo et al. reported the successful design of small seven-residue, Zn<sup>2+</sup>-binding, amyloid-forming peptides to mimic the metalloenzymes in the catalysis of ester hydrolysis, and they reported a significant catalytic efficiency ( $k_{\text{cat}}/K_M$ ) of  $62 \pm 2 \text{ M}^{-1} \text{ s}^{-1}$  for *p*-nitrophenyl acetate (PNPA) hydrolysis.<sup>25</sup> Furthermore, Fukushima synthesized the polypeptide poly-(Asp-Leu-His-Leu-Ser-Leu), which contains the catalytic triad of a serine protease, and showed the formation of a  $\beta$ -sheet structure and the potential hydrolysis on the chiral phenylalanine PNPA.<sup>26</sup> These observations suggest that artificial amyloid-like fibrillar catalysts could be used in the successful design of artificial catalysts with encouraging catalytic activities.

In our previous study, we developed a poly(*N*-isopropylacrylamide) [P(NIPAm)] microgel that anchors the functional group of 1-vinylimidazole as a polymeric catalyst to mimic the catalytic behavior of an enzyme.<sup>27</sup> This study clearly showed that a shorter distance between the functional groups is required for an artificial catalyst to achieve high catalytic activity. Therefore, accurate spatial arrangements are required to achieve higher catalytic activity. In this study, peptides containing the three residues of the classical serine-protease catalytic triad of histidyl, seryl, and aspartyl residues were used to functionalize self-assembled amyloid-like fibrils with enzyme-like catalysis properties, particularly peptide catalysis (PC). We hypothesized that the formation of the  $\beta$ -sheet structure via peptide self-assembly is crucial for achieving catalytic activity because closer and stable binding and catalytic sites are endowed by the  $\beta$ -sheet structure in fibrils. In addition, fibrillar PCs can carry multiple binding sites that are required to accelerate catalytic activities. The hydrolysis of amide bonds, which are more stable than ester bonds, is our major challenge. Hence, we designed peptide sequences that could self-assemble to produce fibrillar PCs to digest amide bonds and performed an enzymatic inhibition assay to confirm the enzyme-like catalysis.

## EXPERIMENTAL SECTION

**Peptide Synthesis.** Peptides were custom synthesized using standard 9-fluorenylmethoxycarbonyl solid-phase peptide synthesis.<sup>28</sup> The peptides were purified using high-performance liquid chromatography (HPLC), and the molecular weights were determined by matrix-assisted laser desorption/ionization-time-of-flight mass spectrometry (MALDI-TOF; see Figure S1).

**Fibril Sample Preparation.** Stock peptide solutions (stock concentration, 2.1 mM) were prepared by dissolving a weighed amount of peptide in growth buffer, 0.1 M Tris-HCl buffer at pH 8 or various buffered solutions (0.1 M glycine-HCl buffer at pH 2, 0.1 M acetate buffer at pH 4 and 6, and 0.1 M carbonate buffer at pH 10 for the pH effect test).<sup>19</sup> The peptide solutions were incubated at 25 °C (additional temperatures of 50 and 70 °C for the temperature effect test) without agitation for 96 h. The incubation time was prolonged for up to 2 weeks for samples that were not able to form fibrils to confirm fibril formation, and it was also prolonged for the fibrillated samples to determine the stability of fibril formation. The peptide solutions were vortexed at 24 h intervals during the incubation period to ensure homogeneous fibril formation. The fibers were then collected by centrifugation at 12000 rpm for 10 min and resuspended in the reaction buffer according to the reaction pH needed for the subsequent experiments.

**Amidolytic Activity Measurements.** Amidolytic activity was determined using 2 mM fibrillated PCs and 0.25 mM L-alanine *p*-nitroanilide in various buffers (as mentioned above) at 25 °C (final volume, 300  $\mu$ L) to determine the effect of pH on the amidolytic

activity. The samples were centrifuged prior to the activity measurement to avoid interference from turbidity during the optical density measurements. The reaction mixtures were prepared in 1 mL Eppendorf tubes and centrifuged at 12000 rpm for 10 min at 25 °C. A 200  $\mu$ L aliquot of the collected supernatant containing the released chromophore, *p*-nitroaniline, was then loaded in a 96-well microtiter plate, and the absorbance at 390 nm was measured using a SpectraMax M3 microplate reader (Molecular Devices, Sunnyvale, CA, U.S.A.). The activity measurements were performed using PC4 concentrations ranging from 0.001–3 mM to determine the effect of concentration on amidolytic activity. Amidolytic activity was measured (as described above) using PC4 that fibrillated at different temperatures (25, 50, and 70 °C) to study the effect of temperature on fibril formation and the effect of the resulting fibrils on the amidolytic activity of PC4, which was measured as described above. Two main types of substrates, monopeptide substrates (L-alanine-*p*-nitroanilide, N-succinyl-L-phenylalanine-*p*-nitroanilide, N<sub>a</sub>-benzoyl-L-arginine-*p*-nitroanilide hydrochloride, L-proline-*p*-nitroanilide trifluoroacetate salt, and L-glutamic acid- $\gamma$ (-*p*-nitroanilide) hydrochloride), and oligopeptide substrates (N-succinyl-Ala-Ala-Ala-*p*-nitroanilide, Ala-Ala-Phe-*p*-nitroanilide, N-benzoyl-Val-Gly-Arg-*p*-nitroanilide hydrochloride, and Gly-Pro-*p*-nitroanilide hydrochloride) were obtained from Sigma-Aldrich Co. (St. Louis, MO) and used to evaluate the substrate specificity of PC4, and the amidolytic activity was measured as described above.

**Inhibition Assay.** The following inhibitors were used in the inhibition assays: phenylmethanesulfonyl fluoride (PMSF) from Sigma-Aldrich Co. and 4-amidinophenylmethanesulfonyl fluoride (APMSF) from Wako Pure Chemical Industries (Osaka, Japan). The effects of the inhibitors on the amidolytic activity of PC4 were determined as described above, although different concentrations (0.5–3 mM) of inhibitors were premixed and incubated with PC4 for 24 h at 25 °C prior to the addition of the substrate L-alanine *p*-nitroanilide.

**Circular Dichroism (CD) Spectroscopy.** The CD spectra were acquired using a JASCO J-820 spectrometer equipped with a temperature controller. The measurements were performed at 25 °C in 10 scans of points every 1 nm at a scan rate of 500 nm per min. Spectra (250–190 nm) were collected in 0.1 cm path length quartz cells with a fixed sample concentration of 10  $\mu$ M (diluted with distilled water). The raw data were processed by smoothing and subtracting the blank according to the manufacturer's specified protocol.

**Atomic Force Microscopy (AFM).** The samples were observed on an AFM (Hitachi AFM5300E, Tokyo, Japan) in air at 25 °C. A 400  $\mu$ m long silicon cantilever with a spring constant of 1.9 N/m was analyzed via dynamic force mode (tapping mode) AFM. A total of 10  $\mu$ L (0.05 mM, diluted with distilled water) of the peptide solution was deposited on freshly cleaved mica surfaces and incubated for 10 min. The buffer and salt components were washed from the surface of the mica with distilled water, and the mica was allowed to dry at room temperature. The height and amplitude images were simultaneously obtained. The calibration of the cantilever tip-convolution effect was performed to obtain the true dimensions of the samples using the methods reported previously.<sup>29,30</sup>

**Congo Red Staining.** A 7 mg/mL stock Congo red (Kanto Chemical Co., Inc., Tokyo, Japan) solution was prepared in 0.1 M Tris-HCl buffer at pH 8 and filtered through a 0.2  $\mu$ m syringe filter immediately prior to use. A total of 10  $\mu$ L of the peptide solution (2 mM PCs) was added to a 0.015 mg/mL (final concentration) Congo red solution and incubated overnight at room temperature. At this stage, a red precipitate was visible. The mixture was mixed well, and the spectrum was recorded from 400 to 700 nm using a SpectraMax M3 microplate reader. The same samples were then used for the microscopic analysis by transferring the solution to an Eppendorf tube and centrifuging at 12000 rpm for 10 min to pellet the stained fibrils. The fibrils were washed with water, resuspended in a small amount of water, and then placed on a glass microscope. The air-dried samples were analyzed under polarized and nonpolarized light using a polarized light microscope (Olympus BX51, Hamburg, Germany).

**Raman Spectroscopy.** Raman spectra were collected using a JASCO NRS-4100 (Tokyo, Japan) coupled with an external 532 nm

laser source and an Olympus optical microscope. Spectra were recorded at a spectral range of 1100–1700 cm<sup>-1</sup> and a resolution of 1 cm<sup>-1</sup>. The exposure time was 5 min, and two spectra were collected. Samples that had been fibrillated for 96 h were then washed with distilled water and collected via centrifugation (12000 rpm for 10 min) for lyophilization. The lyophilized samples were measured in the solid state without further preparation on the gold-coated glass slide to avoid interference from the glass peak in the spectra. Baseline corrections were applied using the software provided by JASCO.

**Wide-Angle X-ray Scattering (WAXS).** Synchrotron radiation WAXS measurements were performed using a BL45XU beamline instrument at SPring-8 (Harima, Japan).<sup>31</sup> The X-ray energy was 12.4 keV (0.1 nm wavelength), and a beam with a 150 × 250 μm<sup>2</sup> (*V* × *H*) was employed. All of the WAXS patterns were recorded with a two-dimensional photon counting imaging detector (Pilatus3X 2M; DECTRIS Ltd., Switzerland). The sample-to-detector distance was approximately 224.1 mm. The exposure time for each scattering pattern was 10 s. The obtained two-dimensional (2D) scattering patterns were processed in the background subtraction and converted into one-dimensional (1D) profiles using the Fit2D software.<sup>32</sup>

## RESULTS AND DISCUSSION

**Peptide Design and Fibril Formation.** The amino acid sequences of the PC were designed based on two characteristics: β-sheet forming propensity and sequence arrangement. We targeted the formation of fibrils, which are rich in β-sheet content. Various studies have suggested that the β-branching of an amino acid side chain induces the formation and stability of β-sheets,<sup>33,34</sup> and the periodicity of amino acids is another major factor that determines the secondary structure of short self-assembling peptides. An interesting report showed that when the periodicity of an amino acid sequence matches the repeat pattern of an α-helix (3.6 residues per turn) or a β-strand (2 residues per turn), the sequence will form the respective secondary structure.<sup>35</sup>

Table 1 summarizes the PC designs used in this study, which are based on the aforementioned characteristics. PC2, PC4, and

**Table 1. Amino Acid Sequences and Isoelectric Points (pI) of the Peptide Catalysts (PCs) Investigated in This Study**

peptide catalyst	amino acid sequence	isoelectric point, pI <sup>a</sup>
PC1	Ac-TTSGHTDTT-NH <sub>2</sub>	5.05
PC2	Ac-TGTHTSTD-T-NH <sub>2</sub>	5.05
PC3	Ac-FFSGHFDF-NH <sub>2</sub>	5.08
PC4	Ac-FGFHFSFDF-NH <sub>2</sub>	5.08
PC5	Ac-AASGHADAA-NH <sub>2</sub>	5.08
PC6	Ac-AGAHASADA-NH <sub>2</sub>	5.08

<sup>a</sup>The pIs are theoretical values determined by ExPASy Compute pI/Mw.

PC6 have a repeating pattern of polar and nonpolar amino acids that should match the structural periodicity required for β-sheet structure formation, and PC1, PC3, and PC5 have a random pattern of polar and nonpolar amino acids that should act as a negative control for a lack of β-sheet structure formation. The nonpolar amino acids of the PC sequences included the residues that favor β-sheet formation, that is, threonine (Thr) and phenylalanine (Phe), which presented higher β-sheet-forming propensities in the model system of Minor and Kim,<sup>33</sup> as well as alanine (Ala), which is one of the residues that constitute the highly repetitive GAGAGS amino acid motifs capable of folding into a β-sheet structure in the crystalline regions of natural silk fibers.<sup>36</sup> Polar amino acids include the residues of the serine protease catalytic triad

(serine-histidine-aspartic acid), which are responsible for the catalytic function of PC via a “charge relay system”, as well as a residue of glycine (Gly) because the backbone NHs of Gly have been reported to stabilize the reaction intermediate known as the oxyanion hole.<sup>37</sup> The terminal groups of all the peptide sequences were neutralized via acetylation and amidation at the N-terminus and C-terminus, respectively. This procedure was used to ensure that the self-assembled fibrils were properly arranged in the parallel/antiparallel pattern by eliminating the unfavorable electrostatic interactions between the polar end groups.<sup>26</sup>

**Solution Structure and Assembly of PCs at Different pH Values.** Polymorphisms are a common feature of many fibrillogenic peptides, such as  $\text{A}\beta_{1-40}$ , insulin, and  $\alpha$ -synuclein.<sup>38,39</sup> For example,  $\alpha$ -synuclein has been shown to predominantly adopt β-sheet or α-helical conformations under different conditions.<sup>40</sup> The structural basis of fibrillogenic peptide polymorphisms can arise from a variety of environmentally dependent growth conditions, including pH, temperature, and salt concentrations. The pH factor has a considerably greater impact on the polymorphism feature of fibrillogenic peptides because different types of peptides have different net charges in the peptide chain and thus produce different patterns of polymorphism.<sup>41</sup> An optimum pH condition also crucially influences the ionizable and hydrophobic side chains of peptide residues to provide the intersheet interactions for β-sheet fibril formation and stabilization.<sup>42</sup>

The ability of our designed PCs to form the target β-sheet fibrils at different pH values was characterized by CD spectroscopy (Figure 1). Surprisingly, all of the sequences that possessed a repeating pattern of polar and nonpolar amino acids, which were predicted to be highly favorable for forming β-sheets (PC2, PC4, and PC6), did not show a β-sheet-like spectrum at any pH except for PC4, which displayed a negative band at approximately 218 nm and a positive band near 195 nm under both acidic (pH 2) and alkaline (pH 8, 10, and 12) conditions with the exception of pH 4 and 6, thus, indicating the presence of a predominant β-strand structure. The predominant β-strand content of PC4 (composition of 93.6%) was estimated to be highest at pH 8 (Table S1), as predicted using the CONTIN method.<sup>43</sup> PC2 and PC6 had a predominant random structure and typical minima near 195 nm for all pH conditions.<sup>44</sup> In addition, the random sequences that were predicted to be less favorable for fibril formation (PC1, PC3, and PC5) displayed a typical random coil CD spectra, although PC3 showed a similar trend as PC4, which had also predominant β-strand structure and presented the highest composition of 54.0% at pH 8; however, β-strand structures were revealed at pH 4 and 6.

Morphological characterizations were performed using AFM to visualize the fibrillar structures of our designed PCs and confirm the presence of β-sheet fibrils. Representative AFM images of the different PCs after incubation and fibrillation at different pH values are shown in Figure 2. Consistent with the CD results, fibril formation was only observed with PC3 and PC4; however, none of the incubation pH values favored fibril formation. As shown in the images taken at pH 4 and 6, aggregates of PC3 and PC4 were mainly observed, which may have been related to the pI values of PC3 and PC4 (Table 1). The estimated pI value of 5.08 is similar to the incubation pH; hence, the pH values close to the pI value of peptide resulted in the formation of amorphous aggregates as previously reported.<sup>45</sup> Interestingly, AFM images of the PC3 and PC4

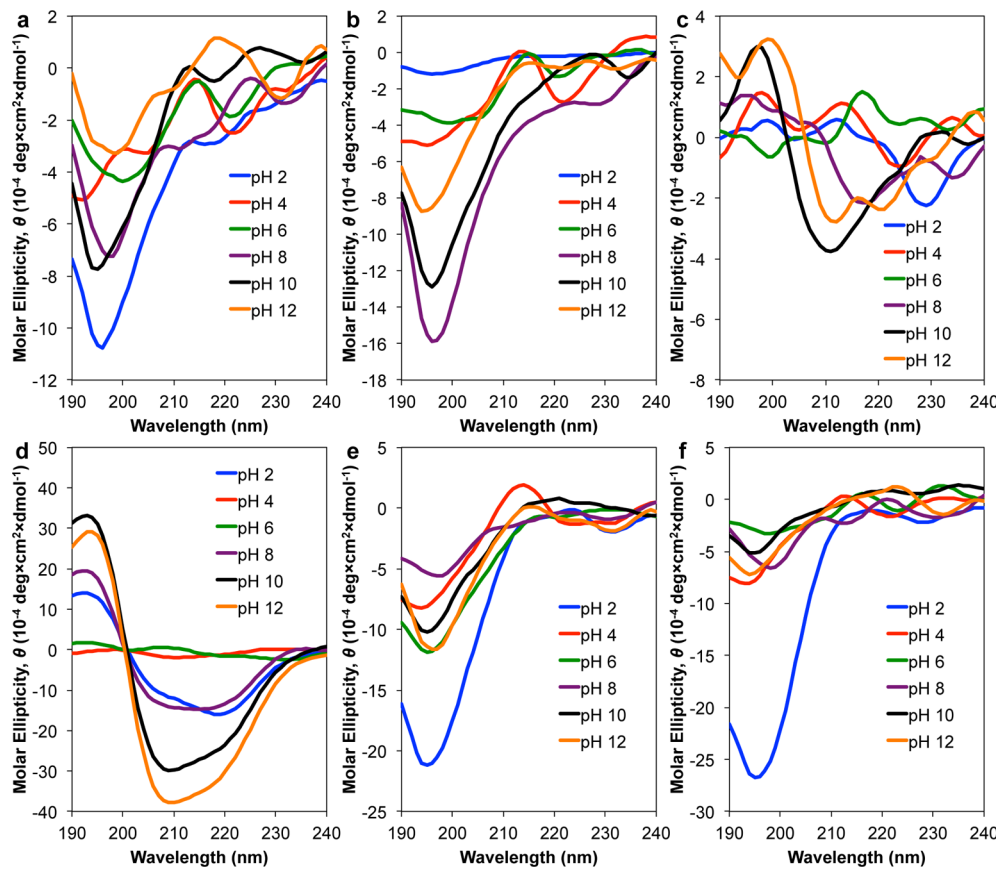


**Figure 1.** CD spectra of different PCs fibrillated at different pH values for 96 h at 25 °C: (a) PC1, (b) PC2, (c) PC3, (d) PC4, (e) PC5, and (f) PC6. The peptide concentration was fixed at 10  $\mu$ M in all conditions.

fibers with different widths could be distinguished at different incubation pH values. The PC3 fibrils formed at pH 2 and 8 exhibited a long and straight fibrillar morphology and had an average width and height of  $140 \pm 5$  nm and  $3.0 \pm 0.5$  nm, respectively, and lengths of up to several micrometers. However, at more alkaline incubation pH values, the fiber width slowly decreased, for example, from  $127 \pm 26$  at pH 10 to  $118 \pm 22$  nm at pH 12, although the morphology of the fibrils remained constant. PC4 also showed similar morphological changes; at pH 2 and 8, and the long straight fibers exhibited an average width and height of  $144 \pm 5$  nm and  $3.1 \pm 0.5$  nm, respectively, whereas from pH 10 to pH 12, the width slowly decreased from  $133 \pm 25$  to  $116 \pm 23$  nm. This result could have been caused by the weak lamination of the soluble fibers at alkaline pH (the lamination and solubility of the PCs will be discussed in subsequent sections). Obvious fibrillar structures were not observed in the other PCs, which only showed oligomeric structures with diameters ranging from 70 to 200 nm.

All the CD spectra and AFM images shown here were taken at 96 h, which produced the most stable form of the fibrillated fibers. Additionally, the PC3 and PC4 fibrils stopped growing and were in the plateau stage at 96 h based on the size distribution pattern collected from the AFM images from the real-time growth study (Figure 3). The fibril morphologies of PC3 and PC4 from 96 h onward remained constant in terms of the width, height, and length of the fibers. Even after 2 weeks of incubation, the appearance of the fibers was easily imaged by AFM, indicating the stability of the fibrillated fibers. The real-time fiber growth study also demonstrated that fiber formation

could not be established for PC1, PC2, PC5, and PC6 at all incubation pH values, even when the incubation period was prolonged for up to 2 weeks (AFM in Figures S2–5. CD in Figures S6–9). Furthermore, the fiber growth study also revealed that the self-assembly of the fibers was initiated at the appearance of oligomers (0 h) to elongated fibers (96 h).

PC3 and PC4 have the same nonpolar amino acid Phe as the  $\beta$ -sheet-forming residue and exhibited the predominant  $\beta$ -strand structure despite the differences in the arrangement of their amino acid sequences. Notably, the key role of the Phe residue in amyloid formation is important, particularly when short fragments (5–12 amino acids) are used for amyloid formation via self-assembly.<sup>46</sup> The involvement of Phe in our designed sequences showed that this aromatic residue may have a significant role in fibril formation by serving as a structural element and contributing to well-known  $\pi$ -stacking interactions. Thermodynamically,  $\pi$ -stacking interactions contribute to the enthalpic change ( $\Delta H$ ) in the free energy of interaction ( $\Delta G$ ), which reduces the energetic barrier and ease the nucleation of fibril formation.<sup>47,48</sup> Different morphologies are commonly observed during fiber formation at the acidic incubation pH, whereas incubations at pH values close to the pI result in the formation of amorphous aggregates. Incubations under alkaline conditions, such as pH 8 and above, are not a common criteria for fiber formation.<sup>49</sup> In our case, the observations of fibril formation from pH 8 to 12 could be explained by the significant role of Phe in easing and strengthening fibril formation in our designed sequences. Another chosen  $\beta$ -sheet-forming residue, Thr, which is at the top of  $\beta$ -sheet-forming propensity, scale did not induce

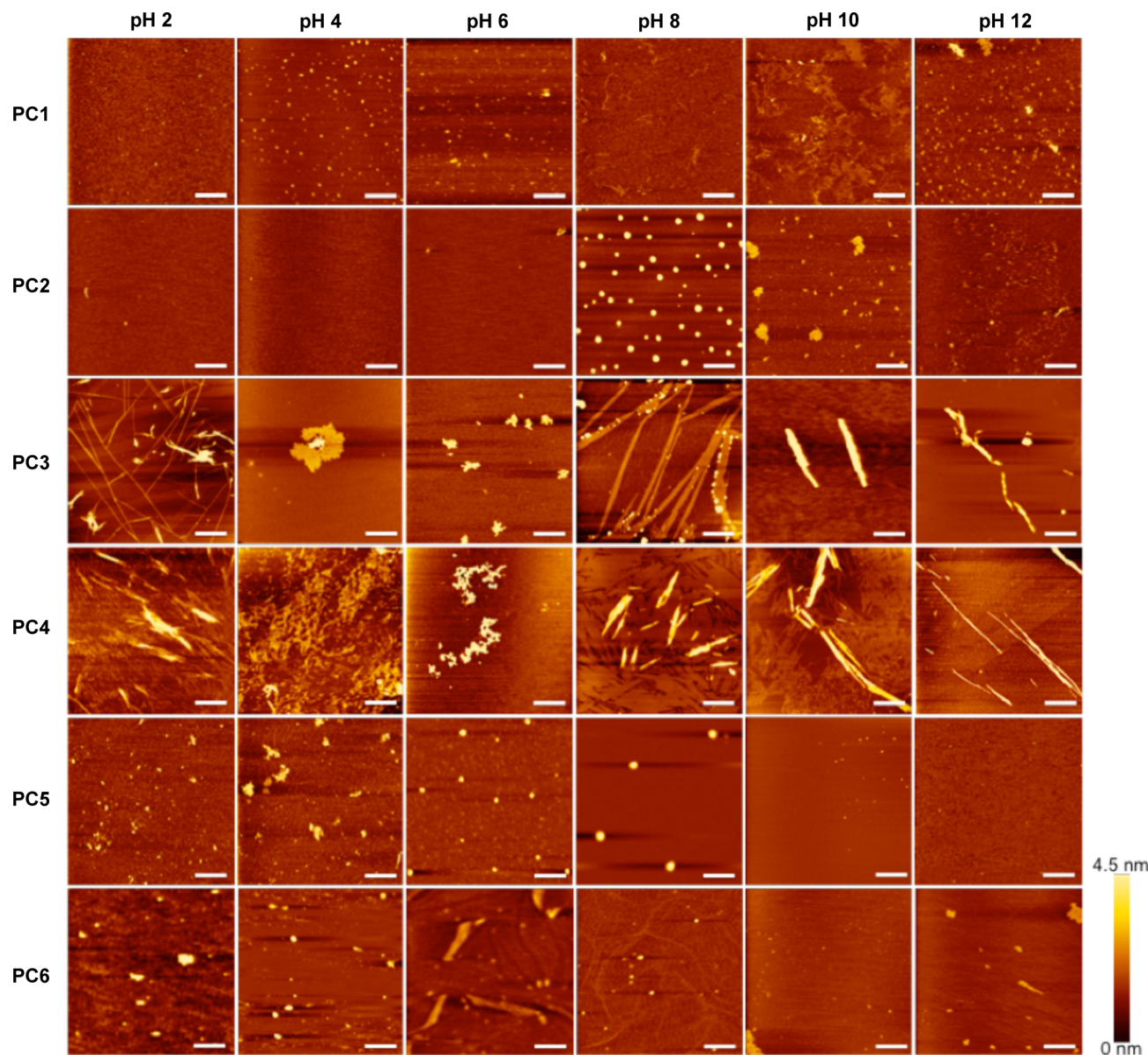


**Figure 2.** AFM images of different PCs fibrillated at different pH values for 96 h at 25 °C; scale bar: 1  $\mu$ m.

noticeable  $\beta$ -strand structures according to the CD spectra. This result indicates that when there is a reduced content of short-chain polar residues (>50% threonine in PC1 and PC2) and other stabilizing forces in a short peptide design, the peptide tends to be too soluble and the intermolecular peptide–water interactions can override the intramolecular interactions of the Thr residues.<sup>45</sup> On the contrary to Thr, the contribution of Ala residues to the  $\beta$ -sheet structure, which is observed in the crystalline regions of natural silk, scarcely contributed to the intermolecular stabilization in our peptide design. This result may have been caused by the short length of our design, which may not form any detectable  $\beta$ -sheet structures via peptide hydrogen bonds; furthermore, the Ala side chain is too short to form significant nonpolar interactions and other side-chain interactions.<sup>50</sup>

**Structural Analyses of the Self-Assembled Fibrils.** Another well-known and important characteristic of amyloid-like fibrils is the occurrence of birefringence after staining with Congo red (CR) dye.<sup>51</sup> PC3 and PC4 were subjected to CR staining to determine whether the self-assembled fibrils are

indeed amyloid-like fibrils. The CR staining method combined with cross-polarizer detection was applied to indicate the presence of typical birefringence as shown in Figure 4a,b. All the observed PC3 and PC4 fibrils that fibrillated at different pH values exhibited a characteristic birefringence in green color, which confirmed the formation of fibrils. The birefringence of our designed peptides was observed under cross-polarized light after CR staining, and it corresponded to that of the positive control *Bombyx mori* silk (cocoon silk; Figure S10). As a negative control, PC3 and PC4 were incubated with the CR dye at pH 4 and 6, and detectable birefringence was not observed under the cross-polarized light. In addition to the CR birefringence assay, a CR spectrophotometric assay was also conducted because the combination of these two assays has been reported to provide more objective results that are less prone to misinterpretation.<sup>52</sup> The CR spectrum was subtracted from the spectra of all of the samples fibrillated at different pH values, and the maximal spectral difference at 540 nm indicated the presence of amyloid-like fibrils (Figure 4c).

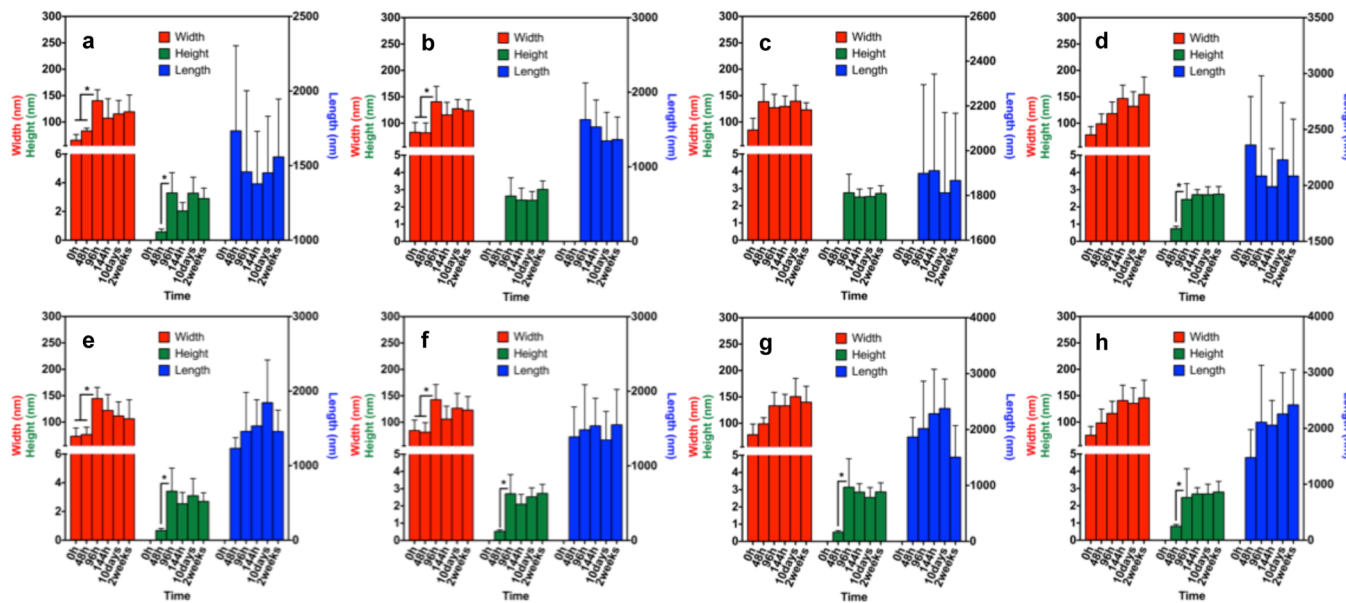


**Figure 3.** Size distributions of the PC3 (a–d) and PC4 fibrils (e–h). Widths, heights, and lengths of the fibrils at pH 2 (a, e), pH 8 (b, f), pH 10 (c, g), and pH 12 (d, h) under different incubation times. All data are the means of replicate tests ( $n = 30$ ). Mean data marked by asterisks (\*) are significantly different (Tukey's HSD test;  $p < 0.05$ ).

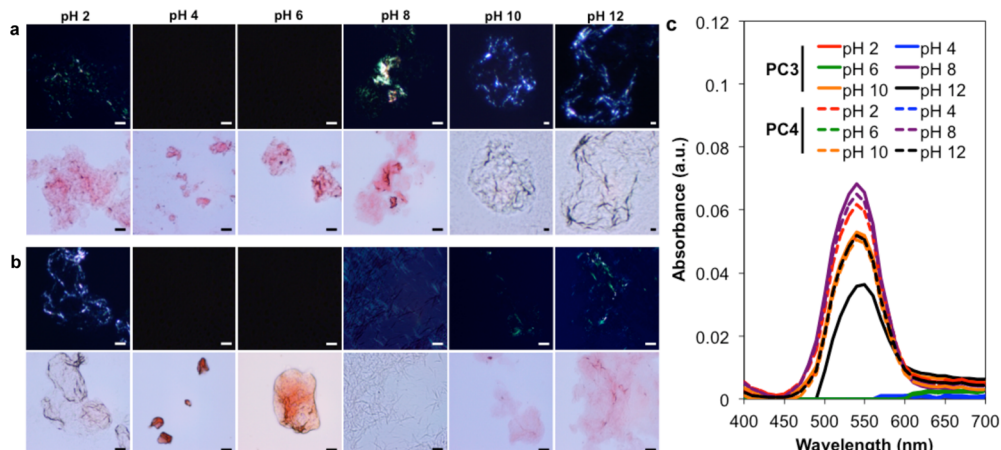


**Figure 4.** Microscopic and spectroscopic analyses of Congo red staining. Polarized (top) and nonpolarized images (bottom) of Congo red (CR)-stained PC3 (a) and PC4 (b) incubated at different pH values. The presence of birefringence from the regions rich in  $\beta$ -sheet fibrils is recognized as a green color. Each scale bar indicates  $10 \mu\text{m}$ . (c) UV-vis spectra of CR-stained PC3 and PC4. A maximal spectral difference at 540 nm indicates the presence of amyloid-like fibrils.

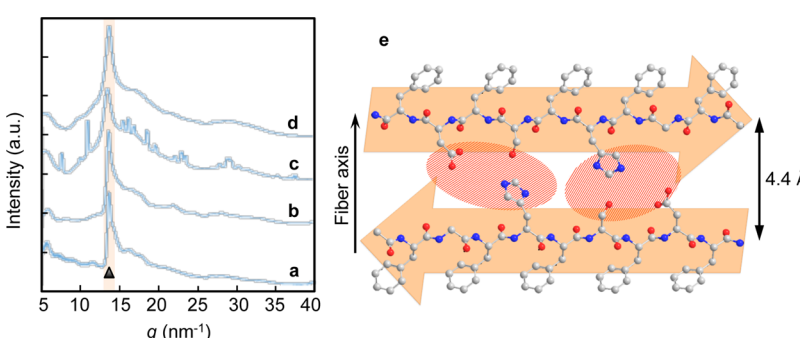


**Figure 5.** 1D WAXS profiles of PC4 (a, b) and PC3 (c, d) prepared at pH 8 (a, c) and pH 10 (b, d). The arrowhead indicates the peak corresponding to the  $4.4 \text{ \AA}$  structure. (e) Schematic illustration showing the structural model of PC4 with a  $\beta$ -sheet structure.

WAXS and Raman spectroscopy were performed to obtain additional structural information on the designed short

peptides. The WAXS profiles of the PC4 fibrils prepared at pH 8 and 10 were similar to the cross- $\beta$  reflections at  $4.4 \text{ \AA}$ ,

which represent typical characteristics of amyloid-like fibrils (Figure 5a,b). The reflection at 4.4 Å represented the distance between chains in the H-bonding direction along the fibril growth axis and indicated that the  $\beta$ -strands were aligned perpendicular to the fibril axis similar to amyloid fibrils. However, the *d*-spacing corresponded to a slightly smaller distance compared with the distance observed in typical amyloid structures (approximately 4.7 Å),<sup>53</sup> which might indicate a closer interaction among  $\beta$ -strands within fibrils formed by short peptides compared with those formed by larger peptides, such as the amyloid peptide. Similarly, the WAXS profile of PC3 fibrils at pH 8 and 10 showed a peak that corresponded to amyloid-like fibrils (Figure 5c,d). Thus, PC3 and PC4 formed  $\beta$ -sheet fibrillar structures as expected.

A typical Raman spectrum in the amide region of PC4 is shown in Figure 6. This spectrum showed a strong amide I

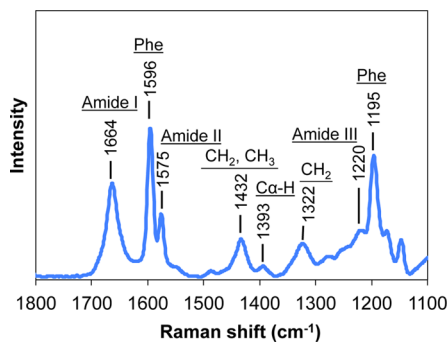


**Figure 6.** Typical Raman spectrum of PC4 fibrils with the main assignments.

band at 1664  $\text{cm}^{-1}$ , which is a marker band for  $\beta$ -sheets, as represented by *B. mori* silk.<sup>54</sup> In addition, reports have indicated that amide III could be correlated with the  $\Psi$  Ramachandran angle in defining the peptide bond secondary structure. A theoretical investigation<sup>55</sup> indicated that the average Ramachandran  $\Psi$  angle of the amide group can be calculated based on the spectral position of the amide III band using the following equation for an anhydrous  $\beta$ -sheet structure:

$$\nu_{\text{amide III}}^{\beta} = 1239 \text{ cm}^{-1} - 54 \text{ cm}^{-1} \sin(\Psi + 26^\circ) \quad (1)$$

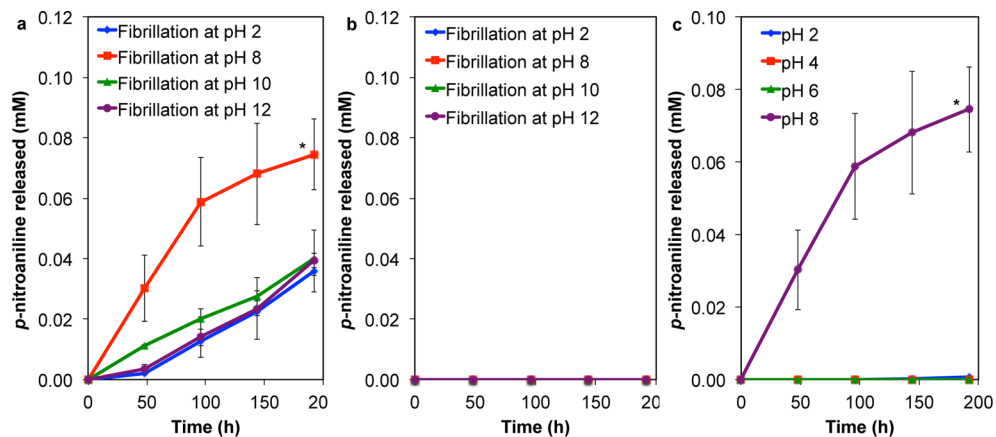


**Figure 7.** Amidolytic activity of (a) PC4 and (b) PC3 on the substrate L-alanine *p*-nitroanilide (0.25 mM) after 96 h of fibrillation at different pH values. The final reaction was performed using 0.1 M Tris-HCl buffer at pH 8 and 25 °C. (c) Amidolytic activity of PC4 at different pH values. All data are the means of triplicate tests, and the mean data marked by asterisks (\*) are significantly different (Tukey's HSD test;  $p < 0.05$ ).

(Phe, Tyr, and Trp) compared with the neutral His species.<sup>56</sup> This phenomenon may occur in the designed peptide sequence because His is surrounded by Phe residues (Phe–His–Phe). The possible involvement of His in the  $\pi$ -stacking interactions during PC self-assembly might disrupt its role as a general base in the hydrolysis mechanism, thereby causing the lower amidolytic activity of PC fibrils prepared at pH 2. We noted that as the incubation pH increased from pH 8 to pH 10 and 12, the PC solution became viscous and transparent because of the increased PC4 solubility at the alkaline pH values (Figure S5a), and these changes may have caused the low amidolytic activity observed at pH 10 and 12.<sup>45</sup> The soluble form of PC4, which did not form fibers, may not favor amidolytic activity. We collected the soluble fraction of the PC4 solution that was incubated at pH 8 for 96 h to test the amidolytic activity and confirm this hypothesis (Figure S11). Consistent with our hypothesis, the amidolytic activity of the soluble PC4 was one-fold lower than the precipitated fibrils prepared at pH 10 and pH 12. The PC3 fibrils prepared at each pH value did not show activity, which may be related to the creation of catalytically inactive fibers by the random sequence arrangement. In addition, the amidolytic activity of the PC4 fibrils was also analyzed under different pH values to optimize the catalytic efficiency (Figure 7c). As expected, PC4 showed the optimal amidolytic activity at pH 8, which corresponds to the observation that the deprotonated His species is important for hydrolytic activity as an active general base.<sup>57</sup> Additional reactions at higher alkaline pH values (e.g., pH 10 and pH 12) were not included in the experiment because those alkaline pH conditions showed significant alkaline hydrolysis of the substrate, which interfered with the amidolytic activity analysis.

**Concentration Effect.** The effects of PC4 concentration on amidolytic activity were evaluated to determine the optimum concentration of PC4 required for amidolytic activity. Concentrations ranging from 0.001 to 3 mM (1.2  $\mu$ g/mL to 3.6 mg/mL) were studied (Figure 8). The amidolytic activity of PC4 was increased as the concentration increased, and the optimum concentration was recorded at 2 mM. An approximately one-fold increase in amidolytic activity was observed in the reaction with 2 mM PC4 compared with the

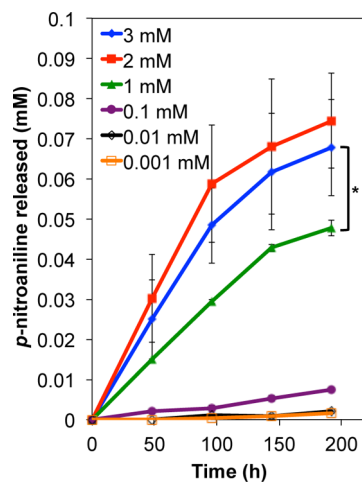


**Figure 8.** Amidase activity of different concentrations of PC4 on the substrate L-alanine p-nitroanilide (0.25 mM) at 25 °C and pH 8. All data are the means of triplicate tests, and the mean data marked by asterisks (\*) are significantly different (Tukey's HSD test,  $p < 0.05$ ).

reaction with 1 mM PC4; thus, we expected that higher activity could be achieved with a higher concentration of PC4. However, the amidolytic activity of 3 mM PC4 remained constant and exhibited the same activity rate as 2 mM PC4, which indicated that PC4 became saturated at a concentration of 2 mM.

**Temperature Effect.** The active site of the proteolytic enzyme is strongly correlated with temperature, which was analyzed to determine its ability to improve catalytic efficiency. In addition, fibril formation, particularly the fibrillation rates and fibril morphologies, are influenced by temperature. We evaluated the effect of temperature on fibril formation and subsequent amidolytic activity. PC4 was characterized at various temperatures using AFM and CD to examine the structural changes induced by different incubation temperatures (Figure 9). Consistent with the reported data, the fibrillation

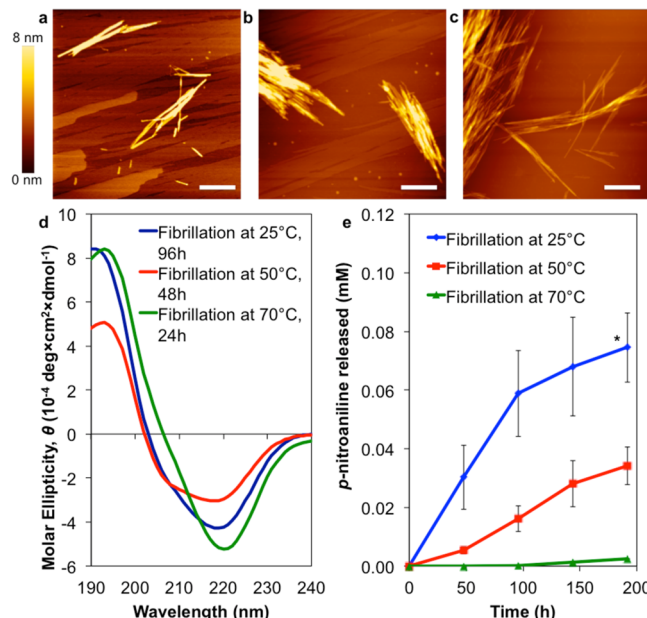


**Figure 9.** Effects of temperature on PC4 fibrillation were evaluated. AFM images of PC4 incubated at different temperatures until stable fibrils were formed (based on the size distribution of PC4 over time) at specific time points: (a) after 96 h of incubation at 25 °C, (b) after 48 h of incubation at 50 °C, and (c) after 24 h of incubation at 70 °C. Scale bar: 1  $\mu$ m. (d) CD spectra show the predominant  $\beta$ -strand structure of PC4 at different time points under different incubation temperatures. (e) Amidase activity of 2 mM PC4 on the substrate L-alanine p-nitroanilide (0.25 mM) at different fibrillation times under different incubation temperatures. The final reaction was performed at 25 °C. All data are the means of triplicate tests, and the mean data marked by asterisks (\*) are significantly different (Tukey's HSD test;  $p < 0.05$ ).

rate of PC4 was greatly improved at incubation temperatures of 50 and 70 °C relative to an incubation temperature of 25 °C. Moreover, the time to stable fibril formation was decreased from 96 h at 25 °C to 48 and 24 h at 50 and 70 °C, respectively (CD in Figure S12 and AFM in Figure S13). This observation could be explained by the activation energy during fiber formation because high temperature environments help maintain the energy required for activation, thus increasing the fibrillation rate.<sup>58</sup> CD measurements also confirmed that the temperature-dependent fibrillation promoted the formation of the  $\beta$ -strand structure of PC4, which exhibited a negative

band at approximately 218 nm and a positive band at approximately 195 nm (Figure 9d). After the stable fibrillation of PC4 at early time points at incubation temperatures of 50 and 70 °C, fibrils were collected for the subsequent amidolytic activity test (Figure 9e). Surprisingly, the activity results suggest that the amidolytic activities of the fibrils prepared at higher temperatures were decreased by one-fold at 50 °C and were almost negligible at 70 °C. This decrease in activity was most likely related to the morphology of PC4 during the packing or lamination steps of  $\beta$ -sheet fibril formation. Incubation temperature has been reported to have a dramatic effect on the final morphology of the formed fibrils.<sup>41</sup> Well-ordered, straight, and occasionally twisted fibrils are common when fibrillation is performed under conditions of slow nucleation. Slow nucleation promotes the formation of laminates because of the collision of diffuse, slow growing fibrils throughout the solution with other growing sheets. Thus, large well-ordered fibril stacks that slowly precipitate over time were obtained via slow nucleation at 25 °C (Figure 2, PC4 at pH 8 incubated for 96 h). In contrast, fast nucleation, which occurs under high incubation temperatures, often produces fibers that appear thinner and more flexible and have considerably less lamination.<sup>59</sup> Therefore, the highly stacked or laminated morphologies of PC4 were considered crucial factors for demonstrating the capability of PC4 to exert amidolytic activity.

**Substrate Specificity Study.** Different types of substrates were evaluated using PC4 and the optimal condition determined above to clarify the reaction mechanism of the PC. Figure 10 shows the amidolytic activities of PC4 on

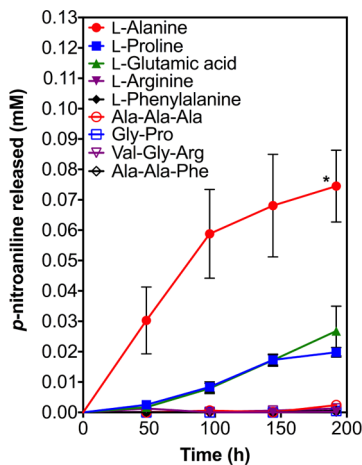


**Figure 10.** Amidase activity of 2 mM PC4 on different types of substrates (fixed concentration at 0.25 mM) after 4 days of incubation at pH 8 and 25 °C. All data are the means of triplicate tests, and the mean data marked by asterisks (\*) are significantly different (Tukey's HSD test;  $p < 0.05$ ).

monopeptide substrates and oligopeptide substrates, such as alanine, proline, glutamic acid, arginine, phenylalanine, alanine trimer, glycine-proline, valine-glycine-arginine, and alanine-alanine-phenylalanine. The catalytic constants were obtained from the hydrolysis of the amide bond linked to the chromophore *p*-nitroaniline. The results showed that the amidolytic activities of PC4 decreased as the bulkiness of the substrate increased because of the attachment of all amino acids. Because L-alanine was the smallest of the tested substrates, PC4 showed the highest amidolytic activity toward L-alanine, whereas when bulkier substrates, such as L-glutamic

acid and L-proline, were used, the amidolytic activity was reduced by approximately 50%. When bulkier substrates with aromatic side chains (L-arginine and L-phenylalanine) and oligopeptide substrates were used, the amidolytic activity was much lower compared with the activity obtained using monopeptide substrates. For example, the amidolytic activity of the succinyl group attached to an alanine trimer in the Suc-(Ala)<sub>3</sub> substrate was almost 30-fold lower than that of the monoalanine substrate. This observation strengthens the conclusion that an increase in the bulkiness of a substrate will lead to a reduction in the amidolytic activity of PC4. Because PC4 has a net negative charge at pH 8 (estimated pI = 5.08), electrostatic interactions occur between PC4 and the positively charged substrate L-arginine. Apparently, the bulkiness of the substrate significantly influenced the electrostatic interaction between the catalyst and substrate. Therefore, the bulkiness of a substrate may restrain the substrate from diffusing between the strands of the  $\beta$ -sheet structure, which is required for subsequent hydrolytic action.

**Inhibition Assay.** To clarify the amidolytic mechanism, we performed an inhibition assay with PC4 using the serine protease inhibitor PMSF, which is commonly used to target and react with the hydroxyl group of the serine residue at the active site of serine protease.<sup>27</sup> As illustrated in Figure 11, PC4

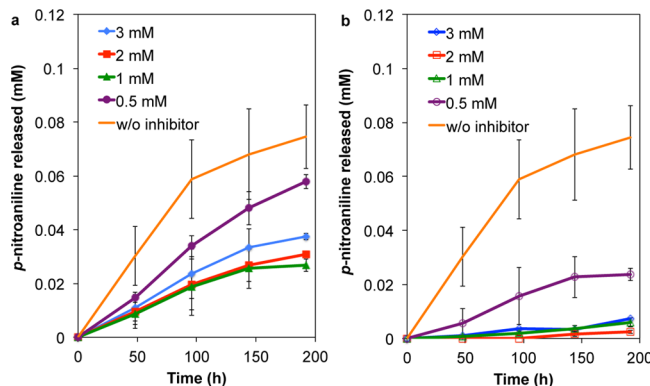


**Figure 11.** Inhibition assay using phenylmethanesulfonyl fluoride (PMSF) (a) and 4-amidinophenylmethanesulfonyl fluoride (APMSF) (b). The effects of the inhibitors on the amidolytic activity of PC4 were determined as described above with the following changes: different concentrations (0.5–3 mM) of inhibitors were premixed and incubated with 2 mM PC4 for 24 h at 25 °C prior to the addition of the substrate L-alanine *p*-nitroanilide (fixed concentration at 0.25 mM) and a 4 day incubation was performed at pH 8 and 25 °C. All data are the means of triplicate tests, and the mean data marked by asterisks (\*) are significantly different (Tukey's HSD test;  $p < 0.05$ ).

was slightly inhibited by a low concentration of PMSF (0.5 mM), although this inhibition did not increase when the concentration of PMSF was increased to 2 mM. Because free seryl residues may have been retained on PC4, indicating that the saturation point had not been reached, we expected that a greater inhibitory effect could be achieved with a higher concentration of PMSF. However, higher concentrations of PMSF (up to 10 mM) tend to precipitate during the inhibition assay and greatly reduce the inhibitory function of PMSF. We used a soluble form of PMSF, APMSF, in the inhibition assays to overcome the drawback of using PMSF. As expected, APMSF showed greater inhibition of PC4, and 1 mM of APMSF was able to inhibit >90% of the amidolytic activity of PC4 because of the higher solubility of APMSF relative to

PMSF. Interestingly, at the same inhibitor concentration (0.5 mM) APMSF produced an approximately 3-fold higher inhibition rate than PMSF. This result suggests that PMSF only binds to seryl residues that are located on the fibril surface and generally does not bind to seryl residues inside the interstrand/intersheet regions of the fibrils. However, the soluble inhibitor APMSF was able to thoroughly diffuse within the interstrand/intersheet regions of the fibrils and exhibited higher affinities and efficient inhibition. The inhibition observed here greatly supports the hypothesis that fibrillar PC4 possesses enzyme-like amidolytic activity that is similar to the activity of serine proteases.

**Estimation of  $k_{\text{cat}}$  Based on the PC Catalytic Site Number.** Implementing the structural framework of the substrate-binding pocket of natural enzymes is important for generating efficient catalysis. Our peptide design aimed to create functional catalytic sites via the self-assembly of a peptide into an antiparallel  $\beta$ -sheet structure (Figure 5e). Compared with the active site of an enzyme, the sites of catalysis for artificial catalysts may not be uniform. Therefore, complications arise when calculating and discussing the kinetics involved in the Michaelis–Menten-type catalysis of artificial catalysts. In the case of fibril-based artificial catalysts, the orientation of the self-assembled fibril structure, which initiates from a simple  $\beta$ -strand to the assembly of  $\beta$ -sheets and amyloid-like fibrils, affects the activity and turnover rate. As shown in Figure 5e, the proposed structural model and hierarchy of assembly based on an antiparallel alignment and  $d$ -spacings determined via Raman spectroscopy and WAXS are applied when calculating the number of catalytic sites for the  $k_{\text{cat}}$  estimation.

We calculated the number of reaction sites according to the methods described in previous reports.<sup>60,61</sup> The estimated antiparallel alignment obtained from Raman spectroscopy suggests that there may be two active sites per pair of  $\beta$ -strands (shaded areas in Figure 5e). Thus, we must determine the number of peptide molecules in the fibril form to identify the number of catalytic sites. To calculate the actual number of PC4 molecules that contribute to amidolytic activity, the yield of the precipitated fibrils was determined according to the weight of the fibrils, and the results were used to calculate the actual number of PC4 molecules that generate amidolytic activity, which was approximately  $83 \pm 11\%$ . Based on the total concentration of peptide molecules (2 mM), approximately 1.66 mM PC4 molecules was used for fibril formation. The number of catalytic sites should be the same as the number of peptide molecules; thus, there were approximately 1.66 mM catalytic sites. The  $k_{\text{cat}}$  of the fibrillar PC4 can be calculated from the Lineweaver–Burk plot, which follows the Michaelis–Menten mechanism with a steady-state approximation:

$$V_0 = \frac{k_{\text{cat}}[C][S]}{K_m + [C]} \quad (2)$$

where  $V_0$  is the initial rate,  $S$  is the substrate,  $k_{\text{cat}}$  is the turnover rate,  $K_m$  is the Michaelis constant, and  $C$  is the concentration of active sites. PC4 generated high amidolytic activity and had a  $k_{\text{cat}}$  of  $8.90 \pm 0.20 \times 10^8 \text{ s}^{-1}$  and a  $K_m$  of  $0.50 \pm 0.02 \text{ mM}$  (Figure S14). Even though this  $k_{\text{cat}}$  value only holds when all of the active sites on the PC4 fibrils are active, the catalytic activity of the fibrillar PC4 was well fit to the Lineweaver–Burk plot, indicating that PC4 is the first enzyme-like peptide catalyst to digest amide bonds.

## CONCLUSIONS

The peptides that anchor the catalytic triads of serine proteases displayed the potential to form efficient artificial catalysts with amidolytic activities at mild pH values. The rational design of a repeating pattern of polar and nonpolar amino acids favors the conversion of short peptides into amyloid-like fibrils via self-assembly. The pH of the fibrillation environment has a crucial effect on the  $pK_a$  of the side chains of the catalytic triads and is important for stable fibril formation. In addition, temperature is an important parameter that controls the self-assembly process and generates highly stacked or laminated morphologies of PC4. The results presented here show that the morphology and stability of fibrils are crucial and represent important factors for demonstrating the capability of PC4 to exert amidolytic activity. The substrate specificity analysis revealed that less bulky substrates are more susceptible to amidolytic activity. Furthermore, the interstrand region of the PC4  $\beta$ -sheet structure contains more active catalytic sites for efficient amidolytic activity relative to the surface. Additionally, the observed amidolytic activities of PC4 were validated using an inhibition assay, which revealed that PC4 can perform enzyme-like amidolytic catalysis and may therefore be referred to as an artificial amidase. The potential of PC4 to form efficient artificial catalysts for amidolytic activities is undeniable, and this study should be of particular value for future studies developing artificial enzymes.

## ASSOCIATED CONTENT

### Supporting Information

The Supporting Information is available free of charge on the ACS Publications website at DOI: 10.1021/acs.biomac.6b01169.

Figure S1. HPLC and MALDI-TOF data of PC in this study. Figures S2–5. AFM images of PC1, 2, 5, and 6 that were fibrillated at different pH values for different times at 25 °C. Figures S6–9. CD spectra of PC1, 2, 5, and 6 that were fibrillated at different pH values for different times at 25 °C. Figure S10. Optical microscopy images of *Bombyx mori* silk were taken under cross-polarized light after staining with Congo red. Figure S11. Amidase activity of soluble PC4 fibers at 25 °C and pH 8. Figure S12. CD spectra of PC4 that was fibrillated at 50 and 70 °C for different times. Figure S13. AFM images and size distributions of PC4 that was fibrillated at 50 and 70 °C at different pH values for different incubation times. Figure S14. Amidase activity of 2 mM PC4 on different concentrations of substrates at 25 °C and pH 8. Table S1. Analyses of the secondary structures of PCs from the CD data (PDF).

## AUTHOR INFORMATION

### Corresponding Author

\*E-mail: keiji.numata@riken.jp.

### Notes

The authors declare no competing financial interest.

## ACKNOWLEDGMENTS

The authors thank Dr. Takaaki Hikima for his technical support in SPring-8 45XU. This work was supported by the RIKEN Biomass Engineering Program (K.N.). Y.-M.W. thanks the

USM Fellowship scheme and the RIKEN International Program Associate for providing financial support.

## ■ REFERENCES

- (1) Schramm, V. L. *Annu. Rev. Biochem.* **1998**, *67*, 693–720.
- (2) Breslow, R. *Science* **1982**, *218*, 532–537.
- (3) Kirby, A. J. *Angew. Chem., Int. Ed. Engl.* **1996**, *35*, 706–724.
- (4) Murakami, Y.; Kikuchi, J.; Hisaeda, Y.; Hayashida, O. *Chem. Rev.* **1996**, *96*, 721–758.
- (5) Suh, J. *Acc. Chem. Res.* **2003**, *36*, 562–570.
- (6) Cramer, F.; Kampe, W. *J. Am. Chem. Soc.* **1965**, *87*, 1115–1120.
- (7) Lehn, J.-M.; Sirlin, C. *J. Chem. Soc., Chem. Commun.* **1978**, 949–951.
- (8) Karlin, K. D.; Haka, M. S.; Cruse, R. W.; Gultneh, Y. *J. Am. Chem. Soc.* **1985**, *107*, 5828–5829.
- (9) D'souza, V. T.; Bender, M. L. *Acc. Chem. Res.* **1987**, *20*, 146–152.
- (10) Anderson, H. L.; Sanders, J. K. M. *J. Chem. Soc., Perkin Trans. 1* **1995**, 2223–2229.
- (11) Overberger, C. G.; Vorcheimer, N. *J. Am. Chem. Soc.* **1963**, *85*, 951–955.
- (12) Atassi, M. Z.; Manshouri, T. *Proc. Natl. Acad. Sci. U. S. A.* **1993**, *90*, 8282–8286.
- (13) Stavrakoudis, A.; Demetropoulos, I. N.; Sakarellos, C.; Sakarellos-Daitsiotis, M.; Tsikaris, V. *Lett. Pept. Sci.* **1997**, *4*, 481–487.
- (14) Lerner, R. A.; Benkovic, S. J.; Schultz, P. G. *Science* **1991**, *252*, 659–667.
- (15) Yin, Y.; Dong, Z.; Luo, Q.; Liu, J. *Prog. Polym. Sci.* **2012**, *37*, 1476–1509.
- (16) Huang, X.; Liu, X.; Luo, Q.; Liu, J.; Shen, J. *Chem. Soc. Rev.* **2011**, *40*, 1171–1184.
- (17) Adamcik, J.; Jung, J.-M.; Flakowski, J.; De Los Rios, P.; Dietler, G.; Mezzenga, R. *Nat. Nanotechnol.* **2010**, *5*, 423–428.
- (18) Loughlin, W. A.; Tyndall, J. D. A.; Glenn, M. P.; Fairlie, D. P. *Chem. Rev.* **2004**, *104*, 6085–6117.
- (19) Numata, K.; Kaplan, D. L. *Biochemistry* **2010**, *49*, 3254–3260.
- (20) Tan, S. Y.; Pepys, M. B. *Histopathology* **1994**, *25*, 403–414.
- (21) Li, C.; Mezzenga, R. *Nanoscale* **2013**, *5*, 6207–6218.
- (22) Bhak, G.; Lee, S.; Park, J. W.; Cho, S.; Paik, S. R. *Biomaterials* **2010**, *31*, 5986–5995.
- (23) Li, D.; Furukawa, H.; Deng, H.; Liu, C.; Yaghi, O. M.; Eisenberg, D. S. *Proc. Natl. Acad. Sci. U. S. A.* **2014**, *111*, 191–196.
- (24) Raynes, J. K.; Pearce, F. G.; Meade, S. J.; Gerrard, J. A. *Biotechnol. Prog.* **2011**, *27*, 360–367.
- (25) Rufo, C. M.; Moroz, Y. S.; Moroz, O. V.; Stöhr, J.; Smith, T. A.; Hu, X.; Degrado, W. F.; Korendovych, I. V. *Nat. Chem.* **2014**, *6*, 303–309.
- (26) Fukushima, Y. *Bull. Chem. Soc. Jpn.* **1996**, *69*, 2269–2274.
- (27) Wong, Y.-M.; Hoshino, Y.; Sudesh, K.; Miura, Y.; Numata, K. *Biomacromolecules* **2015**, *16*, 411–421.
- (28) Fields, G. B.; Noble, R. L. *Int. J. Pept. Protein Res.* **1990**, *35*, 161–214.
- (29) Numata, K.; Kikkawa, Y.; Tsuge, T.; Iwata, T.; Doi, Y.; Abe, H. *Biomacromolecules* **2005**, *6*, 2008–2016.
- (30) Numata, K.; Kikkawa, Y.; Tsuge, T.; Iwata, T.; Doi, Y.; Abe, H. *Macromol. Biosci.* **2006**, *6*, 41–50.
- (31) Numata, K.; Masunaga, H.; Hikima, T.; Sasaki, S.; Sekiyama, K.; Takata, M. *Soft Matter* **2015**, *11*, 6335–6342.
- (32) Hammersley, A. P. *ESRF Internal Report, ESRF97HA02T; Eur. Synchrotron Radiation Facility Internal Rep.*, 1997.
- (33) Minor, D. L.; Kim, P. S. *Nature* **1994**, *367*, 660–663.
- (34) Smith, C. K.; Withka, J. M.; Regan, L. *Biochemistry* **1994**, *33*, 5510–5517.
- (35) Xiong, H.; Buckwalter, B. L.; Shieh, H.-M.; Hecht, M. H. *Proc. Natl. Acad. Sci. U. S. A.* **1995**, *92*, 6349–6353.
- (36) Numata, K.; Kaplan, D. L. *Macromol. Biosci.* **2011**, *11*, 60–64.
- (37) Tsukada, H.; Blow, D. M. *J. Mol. Biol.* **1985**, *184*, 703–711.
- (38) Petvoka, A. T.; Leapman, R. D.; Guo, Z.; Yau, W.-M.; Mattson, M. P.; Tycko, R. *Science* **2005**, *307*, 262–265.
- (39) Dzwolak, W.; Smirnovas, V.; Jansen, R.; Winter, R. *Protein Sci.* **2004**, *13*, 1927–1932.
- (40) Heise, H.; Hoyer, W.; Becker, S.; Andronesi, O. C.; Riedel, D.; Baldus, M. *Proc. Natl. Acad. Sci. U. S. A.* **2005**, *102*, 15871–15876.
- (41) Morel, B.; Varela, L.; Azuaga, A. I.; Conejero-Lara, F. *Biophys. J.* **2010**, *99*, 3801–3810.
- (42) Fraser, P. E.; Nguyen, J. T.; Surewicz, W. K.; Kirschner, D. A. *Biophys. J.* **1991**, *60*, 1190–1201.
- (43) Provencher, S. W.; Glöckner, J. *Biochemistry* **1981**, *20*, 33–37.
- (44) Greenfield, N. J. *Nat. Protoc.* **2007**, *1*, 2876–2890.
- (45) Mayo, K. H.; Ilyina, E.; Park, H. *Protein Sci.* **1996**, *5*, 1301–1315.
- (46) Ageitos, J. M.; Baker, P. J.; Sugahara, M.; Numata, K. *Biomacromolecules* **2013**, *14*, 3635–3642.
- (47) Azriel, R.; Gazit, E. *J. Biol. Chem.* **2001**, *276*, 34156–34161.
- (48) Wiltzius, J. J. W.; Sievers, S. A.; Sawaya, M. R.; Cascio, D.; Popov, D.; Riek, C.; Eisenberg, D. *Protein Sci.* **2008**, *17*, 1467–1474.
- (49) Gosal, W. S.; Morten, I. J.; Hewitt, E. W.; Smith, D. A.; Thomson, N. H.; Radford, S. E. *J. Mol. Biol.* **2005**, *351*, 850–864.
- (50) Shi, Z.; Olson, C. A.; Rose, G. D.; Baldwin, R. L.; Kallenbach, N. R. *Proc. Natl. Acad. Sci. U. S. A.* **2002**, *99*, 9190–9195.
- (51) Puchtler, H.; Sweat, F.; Levine, M. *J. Histochem. Cytochem.* **1962**, *10*, 355–364.
- (52) Nilsson, M. R. *Methods* **2004**, *34*, 151–160.
- (53) Sunde, M.; Serpell, L. C.; Bartlam, M.; Fraser, P. E.; Pepys, M. B.; Blake, C. C. F. *J. Mol. Biol.* **1997**, *273*, 729–739.
- (54) Maiti, N. C.; Apetri, M. M.; Zagorski, M. G.; Carey, P. R.; Anderson, V. E. *J. Am. Chem. Soc.* **2004**, *126*, 2399–2408.
- (55) Mikhonin, A. V.; Bykov, S. V.; Myshakina, N. S.; Asher, S. A. *J. Phys. Chem. B* **2006**, *110*, 1928–1943.
- (56) Liao, S.-M.; Du, Q.-S.; Meng, J.-Z.; Pang, Z.-W.; Huang, R.-B. *Chem. Cent. J.* **2013**, *7*, 44–55.
- (57) Hedstrom, L. *Chem. Rev.* **2002**, *102*, 4501–4523.
- (58) Kusumoto, Y.; Lomakin, A.; Teplow, D. B.; Benedek, G. B. *Proc. Natl. Acad. Sci. U. S. A.* **1998**, *95*, 12277–12282.
- (59) Lamm, M. S.; Rajagopal, K.; Schneider, J. P.; Pochan, D. J. *J. Am. Chem. Soc.* **2005**, *127*, 16692–16700.
- (60) Dobson, C. M. *Trends Biochem. Sci.* **1999**, *24*, 329–332.
- (61) Jimenez, J. L.; Nettleton, E. J.; Bouchard, M.; Robinson, C. V.; Dobson, C. M.; Saibil, H. R. *Proc. Natl. Acad. Sci. U. S. A.* **2002**, *99*, 9196–9201.